$In_3Ti_2Br_9$: Jahn–Teller Unstable Indium(I) and Antiferromagnetically Coupled Titanium(III) Atoms

Richard Dronskowski

Abstract: Dark green crystals of $In_3Ti_2Br_9$ have been synthesized from elemental Ti and molten $InBr_3$ at 450 °C. The X-ray diffractional characterization by means of single-crystal and powder Rietveld refinement reveals a hexagonal crystal structure ($a = 738.2(2)$, $c = 1813.9(3)$ pm; $P6_3/mmc$, $Z = 2$) of $Cs_3Cr_2Cl_9$ type, containing $Ti_2Br_9^{3-}$ dimers and univalent indium cations. Self-consistent, semiempirical band structure calculations show the structural distortions of the two monovalent indium cations to arise from a second-order Jahn–Teller instability. The new compound's magnetic susceptibility and microscopic antiferromagnetic exchange are analyzed by using a Bleaney–Bowers ansatz.

Keywords: antiferromagnetic exchange · crystal structure · indium compounds · Jahn–Teller distortion · titanium compounds

Introduction

Since the original crystal structure determination of $Cs_3Cr_2Cl_9$ in 1957,[1] there has been a constant interest in the crystal structures and physical properties of the family of enneahalodimetalates(III) $A_3M_2X_9$ (A = alkali metal, M = transition metal, X = halogen atom). For example, the, at first sight, counterintuitive trend in the metal–metal internuclear distances[1–3] in the d^3 transition metal series $Cr_2Cl_9^{3-}$ (312 pm), $Mo_2Cl_9^{3-}$ (266 pm), and $W_2Cl_9^{3-}$ (241 pm) has led to a fruitful interplay between the theory of chemical bonding and magnetic phenomena. Since the systematic study of structure[4] and magnetic measurements[5] have now more or less reached maturity for most d^3 transition metal species, the focus of research has recently moved to those compounds containing d^1 metal cations, especially Ti^{3+}, where both spin and angular momentum have to be taken into account in the theoretical treatment of exchange interactions.[6–8]

The synthesis of $In_3Ti_2Br_9$ came unexpectedly as part of a systematic study into the crystal chemistry of monovalent indium in combination with other transition metals. The newly discovered phase contains two interesting features with respect to structure, bonding, and magnetism: First, $In_3Ti_2Br_9$ incorporates two independent, monovalent indium cations, one of which shows the beginning of and the other complete second-order Jahn–Teller instability, which is a very rare phenomenon within crystal chemistry. Second, despite the multitude of physical measurements already conducted on enneahalodimetalates(III), our knowledge of the magnetic properties of Ti^{III} bromides is limited: the only available example is $Rb_3Ti_2Br_9$, the structural data of which have actually never been reported. In the following, we therefore report on the synthesis, crystal structure, electronic structure, and magnetic properties of $In_3Ti_2Br_9$.

[*] R. Dronskowski
Max-Planck-Institut für Festkörperforschung
Heisenbergstrasse 1, 70569 Stuttgart (Germany)
e-mail: drons@simix.mpi-stuttgart.mpg.de

Experimental and Theoretical Techniques

Synthesis: $In_3Ti_2Br_9$ was synthesized in quantitative yield by heating equimolar amounts of freshly prepared $InBr_3$ and elemental Ti within an evacuated glass ampoule at 450 °C for 5 days. $InBr_3$ itself was obtained from aqueous solution [9] and purified by repeated sublimation. Ti metal (Merck, p.a.) was used as purchased. The melt was slowly cooled down to 100 °C at a rate of 2 °C per hour, then to room temperature at 20 °C per hour. Single crystals of $In_3Ti_2Br_9$ crystallized as flat, dark green hexagons with a shiny metallic luster. The new compound is very sensitive to humidity. Thus, all subsequent operations had to be performed either in an argon-filled glove box or handled by Schlenk techniques.

Crystal Structure Analysis: The presence of the hexagonal crystal system was easily apparent from an X-ray powder pattern of microcrystalline $In_3Ti_2Br_9$. A highly resolved Guinier–Simon photograph [10] can be identified by the following characteristic reflections (d value in pm (hkl) relative intensity): 603.0 (101) 13, 369.1 (110) 11, 315.5 (105) 15, 314.8 (201) 19, 302.3 (006) 43, 301.5 (202) 94, 282.6 (203) 100, 261.3 (204) 59, 239.8 (205) 33, 201.1 (215) 11, 184.9 (208) 24, 184.6 (220) 58, 170.5 (209) 16, 157.5 (226) 42, 157.4 (402) 15, 154.5 (403) 19, 150.7 (404) 13, 130.6 (408) 10, 119.8 (422) 18, 118.5 (423) 22, 116.9 (22,12) 19, 116.7 (424) 16, 114.6 (425) 11. To exclude any possible crystallographic error due to twinning and related problems, the subsequent crystal structure determination was performed by two almost independent techniques:

1. *Single-Crystal Technique*: A well-grown single crystal of plate-like shape was mounted on a four-circle diffractometer, and its crystal class was confirmed by axes photographs. Complete sets of intensities at room temperature were obtained by variable-speed, prescan-dependent ω–θ scans. The data sets were then reduced and corrected semiempirically for absorption [11]. The systematic absences indicated space groups $P6_3mc$, $P\bar{6}2c$, and $P6_3/mmc$ but with four weak ($I \approx 5\sigma(I)$) and one stronger ($I \approx 11\sigma(I)$, 003 axis reflection) violation. Since the correct space group, $P6_3/mmc$, was confirmed independently from a powder Rietveld refinement (see below), these violations must be due to multiple and possibly $\lambda/2$ diffraction of the large single crystal (006 is by far the strongest reflection). The structure was solved in $P6_3/mmc$ by use of direct methods (SHELXS-86) [12], while subsequent least-squares full-matrix isotropic and anisotropic refinements (SHELXL-93) [13], with scattering factors of the neutral atoms [14], converged successfully and confirmed the chemical formula. With extinction effects included in the refinement, the R_1 residual [15] dropped to 0.048. On the other hand, the alternative refinements in the

0570-0833/95/0202-0118 $ 20.00+.25/0

two acentric space groups led to wR_2 residuals that were larger by 0.04 ($P6_3mc$) and 0.01 ($P\bar{6}2c$), with up to one order of magnitude larger standard deviations for some of the positional parameters. If the x and y coordinates of the Br positions are allowed to refine independently in $P\bar{6}2c$ (they are coupled according to $y = 2x$ in $P6_3/mmc$), they then prove to be $y = 2x$ symmetry-related within 2σ; this suggests that the best crystallographic description of $In_3Ti_2Br_9$ is indeed a centrosymmetric one ($P6_3/mmc$). It is interesting to note that one particular atom, namely monovalent In(2), was found to sit not on the special Wyckoff position 2*a* (0,0,1/4) but a few picometers off-site. Consequently, In(2)'s site occupation factor (SOF) could only be equal to (or less than) 0.5 in order to avoid meaninglessly short $In^+ - In^+$ distances, and it was fixed at 0.5 to ensure correct stoichiometry up to the last cycle. The validity of this approach was confirmed in a surplus refinement run where the then "free-to-refine" SOF of In(2) converged to 0.505(6). No long-range order for the split occurrence of In(2) around the 2*a* position was apparent from the axes photographs, which did not show any indication of a superstructure. Also, the possibility of a polysynthetic inversion twin could be excluded from an unsuccessful refinement attempt (SHELXL-93). The isotropic displacement factors of the two independent indium atoms are about twice as large as those of the other atoms, although the indium positions are fully occupied (1.004(10) for In(1), $2 \times 0.506(6)$ for In(2)). The reason for this finding, typical for univalent indium, is explained below. The final difference Fourier map was flat, and the strongest residual peak was about 61 pm away from the In(1) atom. Table 1 lists all relevant data of the structure analysis, while Tables 2 and 3 show positional and isotropic displacement as well as anisotropic displacement parameters. Table 4 contains selected interatomic distances [16].

Table 1. Crystallographic data for $In_3Ti_2Br_9$.

Formula; molar mass:	$In_3Ti_2Br_9$; 1159.45 g mol^{-1}
Lattice constants:	$a = 738.2(2)$, $c = 1813.9(3)$ pm, from 25 high angle reflections
Molar volume:	515.7(2) cm^3 mol^{-1}
Space group; formula units:	$P6_3/mmc - D_{6h}^4$ (no. 194); 2
X-ray density; F(000):	4.498 g cm^{-3}; 1012
Absorption coefficient:	13.77 mm^{-1}
Crystal dimensions:	$0.34 \times 0.24 \times 0.17$ mm^3
Instrument:	Enraf-Nonius CAD4 four-circle diffractometer, $Ag_{K\alpha}$, graphite monochromator, scintillation counter
Scan range; type:	$5 < 2\theta < 48°$; $\omega - \theta$ scan
Scan speed:	variable, prescan-dependent
Temperature:	293 K
No. of reflections:	5489, 573 unique
Octants:	$0 \le h \le 10$, $-10 \le k \le 9$, $-26 \le l \le 26$
Absorption correction:	ψ scan with 11 reflections pseudo ellipsoid
Min., max. transmission:	0.070, 0.129
R_{int}; R_σ	0.122; 0.041
Structure solution:	direct methods
Structure refinement:	least-squares method, full matrix
No. of intensities, variables, restraints:	568, 21, 0
Weighting scheme:	$w = 1/[\sigma^2(F_o^2) \times (0.0349\,P)^2 + 14.49\,P]$ $P = (\max(F_o^2, \phi) + 2F_c^2)/3$
Resid. electron density min., max., mean:	-1.07, 1.69, 0.00(24) e Å^{-3}
Extinction correction:	$x = 0.0016(4)$
R_1 ($F_o > 4\sigma(F_o)$):	0.048
wR_2, GOF (all data):	0.156, 1.204

Table 2. Positional parameters and isotropic displacement parameters for $In_3Ti_2Br_9$ (standard deviations in parentheses). For each atom, the first row refers to the single-crystal refinement (U_{eq} in pm^2, a third of the trace of the orthogonalized U_{ij} tensor), and the second row to the powder Rietveld refinement (B_{eq} in Å^2). Note that In(2) exhibits 50% site occupancy.

atom	Wyckoff position	x	y	z	U_{eq}/B_{eq}
In(1)	4*f*	1/3	2/3	0.4396(1)	871(10)
				0.4380(2)	2.6(1)
In(2)	4*e*	0	0	0.2682(3)	648(18)
				0.2667(4)	2.6(1)
Ti	4*f*	1/3	2/3	0.6633(2)	255(7)
				0.6646(4)	0.9(2)
Br(1)	6*h*	0.5029(1)	$2x$	1/4	329(4)
		0.5037(4)			1.18(4)
Br(2)	12*k*	0.1698(1)	$2x$	0.58704(6)	455(4)
		0.1678(4)		0.5876(1)	1.18(4)

Table 3. Anisotropic displacement parameters (pm^2) for $In_3Ti_2Br_9$ (standard deviations in parentheses) according to the single-crystal refinement. The components U_{ij} refer to a displacement factor of the form $\exp\{-2\pi^2(U_{11}h^2a^{*2} + \ldots + 2U_{23}klb^*c^*)\}$.

atom	U_{11}	U_{22}	U_{33}	U_{23}	U_{13}	U_{12}
In(1)	1041(14)	U_{11}	531(13)	0	0	1/2 U_{11}
In(2)	536(13)	U_{11}	872(53)	0	0	1/2 U_{11}
Ti	230(10)	U_{11}	304(15)	0	0	1/2 U_{11}
Br(1)	365(7)	191(7)	373(7)	0	0	1/2 U_{22}
Br(2)	340(7)	521(7)	445(7)	74(3)	$2U_{23}$	1/2 U_{11}

Table 4. Selected interatomic distances (pm) in $In_3Ti_2Br_9$ (standard deviations in parentheses) according to the single-crystal refinement. The shortest (nonbonding) $Br^- - Br^-$ distance is larger than 362 pm.

In(1)	– Br(2)	339.5(2)	(3×)	In(2)	– Br(2)	340.7(4)	(3×)
	– Br(2)	372.3(1)	(6×)		– Br(1)	370.6(1)	(6×)
	– Ti	405.9(4)			– Br(2)	393.9(4)	(3×)
	– Br(1)	406.5(2)	(3×)		– Ti	443.9(2)	(3×)
Ti	– Br(2)	250.7(2)	(3×)	Ti	– Ti	314.4(6)	
	– Br(1)	261.8(2)	(3×)				

2. *Rietveld Powder Technique*: Finely powdered, pure $In_3Ti_2Br_9$ was filled into a 0.3 mm glass capillary and mounted on a calibrated powder diffractometer (STOE Stadi, $Cu_{K\alpha_1}$ radiation). The collection of X-ray data was performed at room temperature (20 °C) by use of a 2θ scan with $10.00 \le 2\theta \le 99.72°$ and a constant step width of 0.02°. The following Rietveld refinement (DBW 9006) [17], utilizing scattering factors of the neutral atoms, was started from the positional parameters of the single-crystal refinement. Using a pseudo Voigt profile function and refining 20 total parameters [18], the residual values and the goodness of fit (GOF) converged to $R_p = 0.028$, $R_{wp} = 0.039$, $R_{Bragg} = 0.023$, and GOF = 1.09 for 202 Bragg reflections (4487 data points). Figure 1 (top) gives an overview of the refinement. The lattice

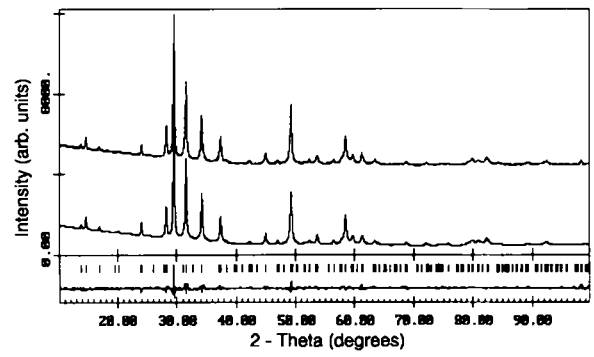

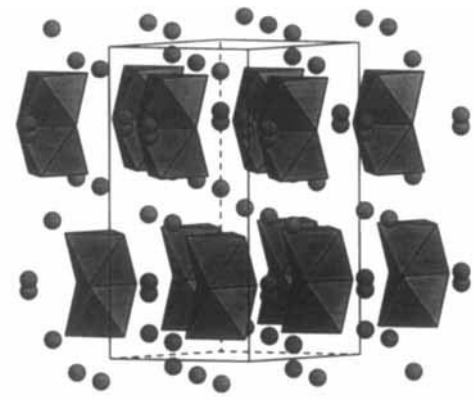

Fig. 1. Top: Rietveld refinement of $In_3Ti_2Br_9$: Depicted are (from top to bottom) measured and fitted diffraction patterns, calculated positions of the Bragg peaks, and the difference between measured and calculated intensities. Bottom: Polyhedral view of the $In_3Ti_2Br_9$ crystal structure, containing dimeric $Ti_2Br_9^{3-}$ units and univalent indium ions (located at around $z = 0$, 1/4, 1/2, and 3/4).

constants extracted from powder, $a = 738.53(3)$ and $c = 1813.5(1)$ pm, are in excellent agreement with the refined lattice constants of the single crystal. Also, the positional parameters (Table 1) are almost exactly the same as those from the single-crystal refinement. In particular, the occurrence of the off-site position for the In(2) atom was fully confirmed. However, due to the better data-to-parameter ratio, the crystallographic accuracy of the single-crystal investigation seems to be slightly (but not much) higher than the one of the Rietveld refinement.

Band Structure Calculations: Charge-self-consistent, semiempirical band structure computations (CSC-EH-TB) [19,20] of $In_3Ti_2Br_9$, with electron correlation effects corrected up to first order and counterintuitive orbital mixing suppressed [21], were based on Slater-type orbitals that had been fitted to either numerical or Herman-Skillman-type atomic wave functions. The calculations followed in all details (basis functions, start and charge-iteration parameters) a general scheme that has already been explained in independent publications [22,23]. Using a modified EHMACC code [24], the eigenvalue problem was solved in reciprocal space at $28\,k$ points within the irreducible wedge of the Brillouin zone. The resulting exchange integrals (after 58 cycles toward self-consistency) and the basis sets used are tabulated in Table 5. All computations were performed under UNIX on a DECstation 5000/133 machine.

Table 5. Slater orbital exponents [38,39], charge-iterated exchange integrals, and quantum mechanical (Mulliken) charges for $In_3Ti_2Br_9$. Note that Ti d orbitals were approximated by double-zeta functions with exponents $\zeta_1 = 4.218$, $\zeta_2 = 1.664$, and weighting coefficients $c_1 = 0.469$, $c_2 = 0.686$.

atom	orbital	ζ	H_{ii} (eV)	charge
In(1)	5s	1.934	−10.955	+0.316
	5p	1.456	−6.127	
In(2)	5s	1.934	−11.069	+0.329
	5p	1.456	−6.221	
Ti	4s	2.617	−7.436	+0.217
	4p	1.190	−4.335	
	3d		−8.392	
Br(1)	4s	2.588	−23.164	−0.140
	4p	2.131	−10.858	
Br(2)	4s	2.588	−22.983	−0.169
	4p	2.131	−10.545	

Magnetic Measurements: A 171 mg sample of selected crystals of $In_3Ti_2Br_9$ was subjected to a susceptibility measurement by use of a Quantum Design MPMS 5.5 Squid susceptometer within a temperature range of 2–300 K at a field strength of 1 Tesla. The diamagnetic influence of the atomic core shells on the molar susceptibilities was corrected using tabulated values [25] for Ti^{3+} and Br^- while the (interpolated) value for In^+ (-23×10^{-6} emu mol^{-1}) was taken from a previous investigation [26].

Electrical Conductivity: Microcrystalline material of $In_3Ti_2Br_9$, covered by a protective helium atmosphere, was pressed to a pellet and contacted according to the four-probe technique. The geometry factor was taken into account by the formula of van der Pauw [27]. Cooling and heating curves were measured between 15–300 K at a constant current of 10 nA.

Results and Discussion

Geometric and Electronic Structure: The crystal structure of $In_3Ti_2Br_9$ (Fig. 1, bottom) belongs to the $Cs_3Cr_2Cl_9$ structure type in which isolated M_2X_9 complex anions, in this case $Ti_2Br_9^{3-}$ units, are stacked in a sheet-like manner around $z = 1/4$ and 3/4. Univalent indium cations fill the remaining voids at $z = 0$ and 1/2 (the position of In(1)) and at $z \approx 1/4$ and 3/4 (the position of In(2)). The corresponding density-of-states (DOS) curve for this particular compound is given in Figure 2, with the local indium contributions emphasized in black. The latter atoms mix mostly into the region between −13 and −8.5 eV, which is clearly dominated by the Br 4p orbitals; the strongly Br-centered, almost core-like 4s bands below −23 eV are not shown. The shape of the local indium DOS curve reflects strong 5s character, and, besides some small indium 5p contribution here, it is only the virtual DOS above −3 eV that may be described as being truly In 5p-centered. The Fermi level (dashed line) cuts through a strongly spiked region of mostly Ti 3d/4s and Br 4p character, but there is also a little mixing in of In 5s. Moreover, there are some fairly localized, empty Ti 3d combinations between −6 and −4 eV, resulting from the particular crystal field of the $Ti_2Br_9^{3-}$ unit. As expected, the electrical conductivity measurements reveal that $In_3Ti_2Br_9$ is a typical intrinsic semiconductor with a band gap of 1.0 eV. The non-zero theoretical DOS at the Fermi energy may thus be understood to originate from a critical flaw, namely, that the calculated HOMO–LUMO gap is too small.[28] Together with the additional Gaussian broadening (0.05 eV) used for graphically generating the DOS, it has finally led to an artificial closing of the band gap.

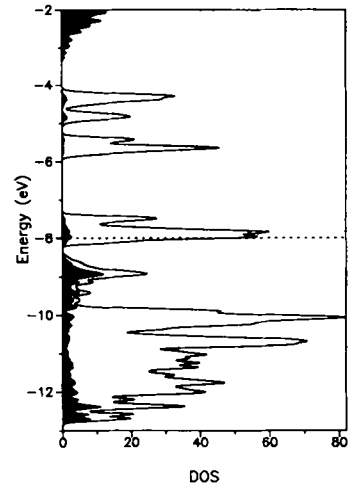

Fig. 2. CSC-EH-TB semiempirical density-of-states (DOS) of $In_3Ti_2Br_9$ with In contributions emphasized in black.

The two coordination polyhedra of the monovalent indium ions are given in Figure 3. The In^+-Br^- bonds are long (which is quite typical for In^+), and the range of bond lengths is similar for In(1) (340–407 pm) and In(2) (341–394 pm). However, the two 12-fold coordination polyhedra differ significantly: while the top-to-bottom stacking order of the coordinating Br^- may be described as following a ("cubic") ABC order for In(1), the

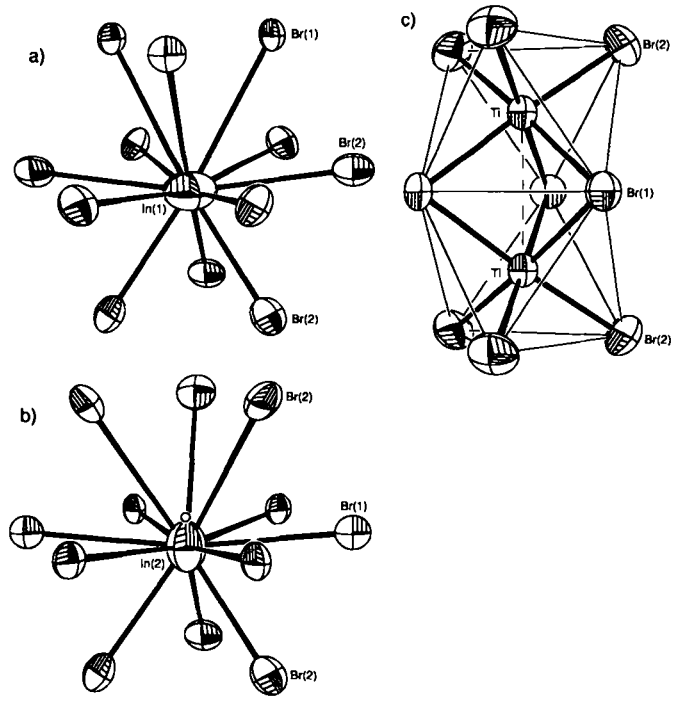

Fig. 3. a) Perspective views in $In_3Ti_2Br_9$ (the ellipsoids enclose 70% of the electrons' spatial probability): a) $In(1)^+$ coordination by Br^- ions. b) $In(2)^+$ coordination by Br^- ions. The small open circle indicates the alternative position available to $In(2)^+$. c) Ti^{3+} coordination by Br^- ions. $Ti^{3+}-Br^-$ bonds are represented by thick lines and the edges of the two connecting octahedra by thin lines; the $Ti^{3+}-Ti^{3+}$ bond is indicated by a dashed line.

0570-0833/95/0202-0120 $ 20.00+.25/0 Chem. Eur. J. 1995, 1, No. 2

("hexagonal") order is ABA for In(2). In other words, In(1) lies inside an approximate cuboctahedron, whereas In(2) is coordinated in a roughly disheptahedron-like manner (sometimes also called "twinned cuboctahedron" in the literature).

As was already mentioned above, In(2) lies slightly off-site from Wyckoff position 2*a*; it moves away from the plane of the six Br(1) atoms (Fig. 3b). The off-site displacement is 33.1(5) pm on the basis of the single-crystal refinement, while the Rietveld powder refinement yields a value of 30.3(5) pm. Such structural distortion has never been reported in isotypic structures containing alkali cations rather than In^+, so the following questions arise: What is the origin of this distortion and why is it observed in the present compound? The answers lie in the In^+-Br^- bonding, which is analyzed by means of crystal orbital overlap population (COOP) plots (Fig. 4: In(1), top left; In(2), top right). The bonding patterns are similar for In(1) and In(2) and common to all known In^+-Br^- combinations within crystalline solids.[22,23] Besides the bonding levels below −10 eV, there is a neighboring, strongly antibonding region at higher energies, which results from the out-of-phase combination between indium 5s and bromine 4p orbitals. Integrated up to the Fermi level, the average overlap populations are 0.070 and 0.074 for In(1) and In(2), respectively, which is quite low, although normal when compared, for example, to the related chemical bonding in the reduced binary indium bromides. A similar bonding cannot be found for alkali metal salts, because of the absence of an almost doubly filled s valence shell.

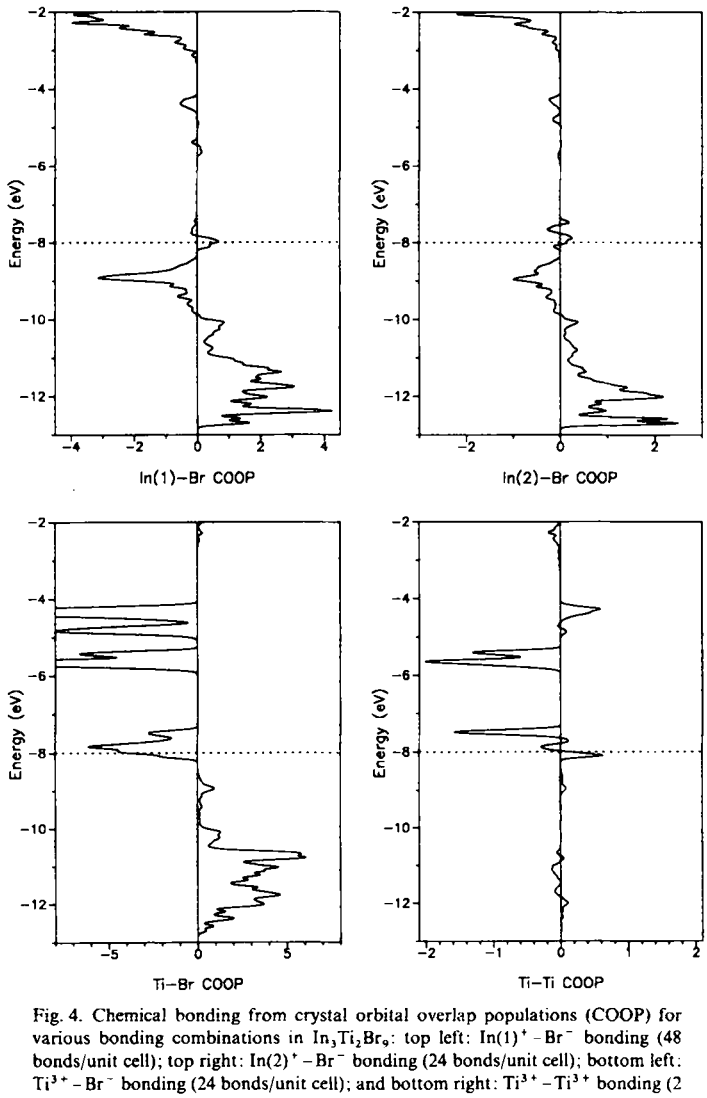

Fig. 4. Chemical bonding from crystal orbital overlap populations (COOP) for various bonding combinations in $In_3Ti_2Br_9$: top left: $In(1)^+-Br^-$ bonding (48 bonds/unit cell); top right: $In(2)^+-Br^-$ bonding (24 bonds/unit cell); bottom left: $Ti^{3+}-Br^-$ bonding (24 bonds/unit cell); and bottom right: $Ti^{3+}-Ti^{3+}$ bonding (2 bonds/unit cell).

Because of the antibonding interactions at the frontier bands, the weak In^+-Br^- bonding leads to a very soft crystal potential at the indium site; thus, atomic vibrations of In^+ require extraordinarily small activation energies. This is reflected in the large room-temperature displacement factors that were mentioned in the Experimental Section. Also, the weak bonding makes any In^+-Br^- coordination polyhedron electronically susceptible to structural distortions.

Semiempirical band structure investigations[22] inspired the first ab initio MO calculations. These demonstrate that highly symmetrical In^+-Br^- polyhedra are excellent candidates for Jahn-Teller instabilities of second order such that In^+ moves away from the polyhedron's center with a lowering of the total energy; the expected drift is 30–60 pm.[29] Such a structural distortion involves a mixing of formerly unoccupied indium 5p levels into the occupied band region, and the energy gain would be rather small. As a consequence, the first observation of such an effect was only made quite recently in a crystallographic low-temperature (90 K) investigation on In_4Br_7, which showed a structural displacement of around 40 pm for one monovalent indium cation.[30]

The split position of In(2) found in $In_3Ti_2Br_9$ represents the first example for a second-order Jahn-Teller effect for In^+ at room temperature. Comparing the In(1)–Br with the In(2)–Br COOP plots, it can be clearly recognized that the antibonding spike at around −9 eV is smaller for In(2) than for In(1), a result of the slight off-site position of In(2), which lowers the total energy. This behavior is also reflected in the specific 5p population ratios of the monovalent indium cations. While the $p_{x/y}:p_z$ ratio is 1:1.04 for In(1), a slightly larger ratio of 1:1.10 is found for In(2); thus, the additional contribution of a $5p_z$ orbital drives the structural distortion along the atomic *z* axis, parallel to the hexagonal *c* axis. It is surprising that such a nonclassical effect seems to be mirrored by a purely empirical (and possibly classical) description.[31] Based on the recently evaluated optimum bond length–bond strength parameter (r_0 = 266.7 pm) for the In^+-Br^- combination,[22] the empirical valences are 0.83 and 0.86 for In(1) and In(2), respectively. However, if In(2) were still at the Wyckoff position 2*a* (with bond lengths of 6 × 366.8 and 6 × 369.1 pm), it would then have a lower bond-order sum of only 0.78, which might be interpreted as indicating a structural instability.

The question arises as to why a similar structural displacement is not observed for In(1). After all, its In^+-Br^- overlap population and its bond-order sum are roughly 6 and 4% smaller than those of In(2), so that a structural distortion might also be possible. Indeed, a comparison of In(1)'s anisotropic displacement parameters $U_{11/22}:U_{33}$ shows that the electron density of In(1) is about two times more diffuse in the *ab* hexagonal plane than along the hexagonal axis. In other words, In(1) also tends to move away from its Wyckoff position 4*f*, not along *c* but along *ab*. Although it is not yet crystallographically justified to represent In(1) with a number of split positions circling around the high-symmetry site, the resolution of the single-crystal refinement (hard $Ag_{K\alpha}$ radiation) is good enough to display (Fig. 3a) the tendency of In(1) to move in the plane of the six Br(2) atoms in the above sense.

In short, the crystal structure of $In_3Ti_2Br_9$ incorporates two examples of second-order Jahn-Teller instabilities for monovalent indium cations: one that is complete (In(2)), having broken

the local symmetry along c such that the bond lengths to the identical top and bottom bromine atoms are no longer degenerate, and one (In(1)) that is significantly smaller, reducing the local symmetry along ab because the top and bottom bromine atoms are already different for reasons of space group symmetry.

Figure 3c shows the atomic environment of the two equivalent, trivalent titanium cations within the $Ti_2Br_9^{3-}$ unit. Ti^{III} is coordinated by six bromine anions with an average bond length of 256.3 pm. Surprisingly, there is only one $Ti^{3+}-Br^-$ bond length available in the literature for comparison; the crystal structure refinement of $TiBr_3$ yielded an almost undistorted octahedron with 258 pm as its mean bond length.[32]

The COOP analysis of the $Ti^{3+}-Br^-$ bonding (Fig. 4, bottom left) shows that the bonding levels are mainly in the Br 4p-dominated region, but that there is also an antibonding regime just above -8.5 eV. The latter region, mostly centered on Ti 3d, contains the single remaining electron of Ti^{III}. It is this additional electron that weakens the $Ti^{3+}-Br^-$ bond to a certain extent—the average overlap population is 0.426—and one might expect that there is a tendency for Ti^{III} to release the electron and so become oxidized to Ti^{IV}, in harmony with the well-known chemical sensitivity of Ti^{III} compounds.

Closer inspection of the Ti^{3+}/Br^- octahedron reveals that the bonds between Ti^{III} and the Br(2) atoms are about 11 pm shorter than between Ti^{III} and the Br(1) atoms.[33] In an alternative description of this arrangement, the titanium atoms do not occupy the centers of the octahedra where they would experience a $Ti^{3+}-Ti^{3+}$ contact of 295.6 pm, but rather "move apart" until they are separated by 314.4 pm. A naive electrostatic interpretation would be to assume that a cation–cation repulsion is responsible for this increased separation; however, the COOP bonding analysis (Fig. 4, bottom right) shows that this assumption is not valid.[34] On the contrary, there is a weak metal–metal bond with an average overlap population of 0.043. The bonding arises almost solely from the additional electron of Ti^{III}, and it is very sharply localized in energy at about -8.1 eV. The presence of such an interaction may be illustrated by a molecular-orbital model calculation[35] (Fig. 5). The weak $Ti^{3+}-Ti^{3+}$ bond length is 314.4 pm, mainly because of the optimization of the $3d_{z^2}-3d_{z^2}$ overlap, which competes with $Ti^{3+}-Br^-$ interactions. In addition, the overall MO shape means that there are only antibonding $Ti^{3+}-Br^-$ effects operating in this highest occupied level or band, making the wave function a possible target for oxidation. Interestingly enough, the corresponding bisoctahedral structural unit $Ti_2Br_9^-$, incorporating tetravalent titanium cations, exists and has been crystallographically characterized; the $Ti^{4+}-Ti^{4+}$ distance is about 343 pm.[36]

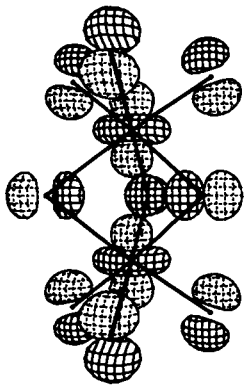

Fig. 5. HOMO (at around -8.1 eV) of a $Ti_2Br_9^{3-}$ molecular anion. The surface value of the wave function is 0.030. For clarity, atomic contributions have been contracted by a factor of 1.5.

Magnetism: The structural and bonding analysis suggests that there may be a magnetic interaction between the two neighboring Ti^{3+} ions. With only one spin present on each of the metal centers, an antiferromagnetic interaction J, for example, would result in a spin-singlet dimer ground state and a spin-triplet dimer excited state that is $2J$ higher in energy. Chemical terminology would designate such a spin-singlet ground state as the above-mentioned two-electron two-center single bond. The underlying (magnetic) Hamilton operator would then be given by Equation (a). Indeed, the corresponding magnetic susceptibility

$$\boldsymbol{H} = -2J\boldsymbol{S}_1\boldsymbol{S}_2 \qquad \text{(a)}$$

curve of $In_3Ti_2Br_9$ exhibits both a very small Curie tail at low temperatures (≤ 30 K) due to paramagnetic impurities as well as a truly non-Curie course above 50 K that is highly characteristic of such magnetically coupled dimers (Fig. 6). An excellent numerical treatment of materials of this kind goes back to the

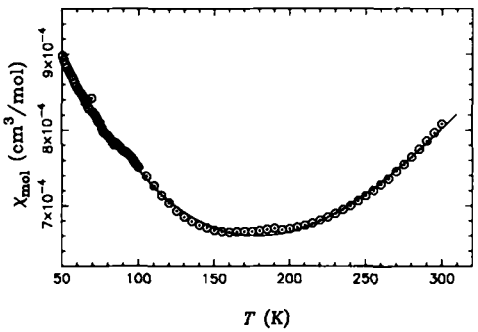

Fig. 6. Molar susceptibility as a function of the temperature for $In_3Ti_2Br_9$ at a field strength of $H = 1$ Tesla. The solid curve represents the Bleaney–Bowers fit for temperatures above 90 K.

classic contribution of Bleaney and Bowers[37] in which the isothermal magnetic susceptibility per mol of dimers χ_{mol} (equivalent to one mol of $In_3Ti_2Br_9$ in the present case) is given by Equation (b). The magnetic data can be nicely fitted

$$\chi_{mol} = \frac{2Ng^2\mu_B^2}{3k_BT}\left\{1 + \left(\frac{1}{3}\right)\exp\left(\frac{-2J}{k_BT}\right)\right\}^{-1} \qquad \text{(b)}$$

to this equation. If the g value is set to 2.00, an approximate interaction energy J/k_B of about -620 K (or roughly 430 cm^{-1}) is obtained for the high-temperature data above 90 K, the region where the singlet–triplet excitation becomes increasingly significant. This value may be compared with that for $Cs_3Ti_2Cl_9$ obtained from single-crystal magnetic studies (about 525 cm^{-1}),[6] and with another value that is also based on an effective Hamiltonian theory (roughly 500 cm^{-1}).[7] The slightly lower value found for the bromide agrees well with the related observation that intradimer exchange decreases in isostructural Cr compounds in the order Cl → Br → I; this parallels the stepwise weakening of metal–metal overlap.[5] Also, inelastic neutron scattering data on the isostructural phase $Rb_3Ti_2Br_9$ point in the same direction in that they indicate the first excited levels to lie around 350 cm^{-1}.[8]

The paramagnetic impurities detected at low temperatures are very probably due to unpaired Ti^{3+} ions (broken dimers) although there may also be traces of Fe^{3+} present in the sample. Assuming one unpaired spin on each of these contaminants, the Curie term of the Bleaney–Bowers fit indicates the presence of 7% impurities. Thus, the measured sample behaves as if every dimer site would carry an additional permanent magnetic moment of roughly $0.19\,\mu_B$.

Acknowledgements: The author would like to thank Dr. Horst Borrmann for the careful single-crystal X-ray data collection, Mrs. Eva Brücher for the susceptibility measurement, Mrs. Nicola Weishaupt for the electrical conductivity measurement,

0570-0833/95/0202-0122 $ 20.00+.25/0

as well as Dr. Richard Reisser and Dr. Reinhard K. Kremer for sharing their expertise on magnetic dimer coupling. The author also gratefully acknowledges generous support by Prof. Dr. Arndt Simon and further financial support by the Fonds der Chemischen Industrie.

Received: December 11, 1994 [F34]

[1] G. J. Wessel, D. J. W. IJdo, *Acta Crystallogr.* **1957**, *10*, 466.
[2] R. Saillant, R. B. Jackson, W. E. Streib, K. Folting, R. A. D. Wentworth, *Inorg. Chem.* **1971**, *10*, 1453.
[3] W. H. Watson, J. Waser, *Acta Crystallogr.* **1958**, *11*, 689.
[4] R. Stranger, I. E. Grey, I. C. Madsen, P. W. Smith, *J. Solid State Chem.* **1987**, *69*, 162.
[5] B. Leuenberger, H. U. Güdel, P. Fischer, *J. Solid State Chem.* **1986**, *64*, 90.
[6] B. Briat, O. Kahn, I. Morgenstern-Badarau, J. C. Rivoal, *Inorg. Chem.* **1981**, *20*, 4193.
[7] M. Drillon, R. Georges, *Phys. Rev. B* **1982**, *26*, 3882.
[8] B. Leuenberger, H. U. Güdel, A. Furrer, *Chem. Phys. Lett.* **1986**, *126*, 255.
[9] F. Ensslin, H. Dreyer, *Z. Anorg. Allg. Chem.* **1942**, *249*, 119.
[10] A. Simon, *J. Appl. Cryst.* **1970**, *3*, 17.
[11] A. C. T. North, D. C. Phillips, F. S. Mathews, *Acta Crystallogr. Sect. A* **1968**, *24*, 351.
[12] G. M. Sheldrick, *Acta Crystallogr. Sect. A* **1990**, *46*, 467.
[13] G. M. Sheldrick, *J. Appl. Cryst.* in preparation.
[14] *International Tables for Crystallography*, Vol. C (Ed.: A. J. C. Wilson), Kluwer Academic Publishers, Dordrecht, **1992**.
[15] R_1 is only for comparison with conventional structure factor F refinements. Note that SHELXL-93 refines against F^2 in order to minimize the so-called wR_2 residual. The latter is indeed based on F^2 and statistically about twice as large as values based on F. The definitions are:

$$wR_2 = \sqrt{\sum[w(F_o^2-F_c^2)^2]/\sum[w(F_o^2)^2]}$$

$$R_1 = \sum||F_o|-|F_c||/\sum(F_o)$$

[16] Further details of the crystal structure investigation are available on request from the Fachinformationszentrum Karlsruhe, D-76344 Eggenstein-Leopoldshafen (Germany), on quoting the depository number CSD-58822.
[17] Program for Rietveld Analysis of X-Ray and Neutron Powder Diffraction Patterns: DBW 9006 (rel. 8.4.91); School of Physics (R. A. Young), Georgia Institute of Technology, Atlanta, GA 30322 (USA).
[18] In detail, these were 1 zeropoint parameter, 5 parameters for reflection shape, 1 parameter for preferred orientation, 1 asymmetry parameter, 1 overall scale parameter, 2 parameters for lattice constants, 6 spatial parameters, and 3 isotropic displacement parameters.
[19] R. Hoffmann, *J. Chem. Phys.* **1963**, *39*, 1397.
[20] S. P. McGlynn, L. G. Vanquickenborne, M. Kinoshita, D. G. Carroll, *Introduction to Applied Quantum Chemistry*, Holt, Rinehart and Winston, New York, **1972**.
[21] J. H. Ammeter, H.-B. Bürgi, J. C. Thibeault, R. Hoffmann, *J. Am. Chem. Soc.* **1978**, *100*, 3686.
[22] R. Dronskowski, *Inorg. Chem.* **1994**, *33*, 6201.
[23] R. Dronskowski, *Inorg. Chem.* **1994**, *33*, 5927.
[24] QCPE program EHMACC by M.-H. Whangbo, M. Evain, T. Hughbanks, M. Kertesz, S. Wijeyesekera, C. Wilker, C. Zheng, R. Hoffmann.
[25] P. W. Selwood, *Magnetochemistry*, 2nd ed., Interscience Publishers, New York, **1956**.
[26] R. Dronskowski, Ph.D. Thesis, Universität Stuttgart, **1990**.
[27] L. J. van der Pauw, *Philips Res. Rep.* **1958**, *13*, 1.
[28] A molecular orbital calculation of a $Ti_2Br_9^{3-}$ unit results in a HOMO–LUMO gap of roughly 0.2 eV on that specific theoretical level.
[29] K. Wu, R. Dronskowski, unpublished results.
[30] R. Dronskowski, *Angew. Chem.* in press.
[31] I. D. Brown, D. Altermatt, *Acta Crystallogr. Sect. B* **1985**, *41*, 244.
[32] S. I. Troyanov, V. B. Rybakov, V. M. Ionov, *Zh. Neorg. Khim.* **1990**, 35, 494; *Russ. J. Inorg. Chem.* **1990**, *35*, 882.
[33] It is interesting to note that the two independent Br atoms are truly different species with respect to their electronic behavior. For example, a look at the Mulliken charges (Table 5) shows that Br(2) is about 20% more highly charged than Br(1).
[34] Also, a structural comparison of $Cs_3Y_2I_9$, $Cs_3Zr_2I_9$ (Zr^{3+}–$Zr^{3+} \approx 313$ pm), and other isotypic phases established that cation–cation repulsion does not play a major role in the crystal chemistry: D. H. Guthrie, G. Meyer, J. D. Corbett, *Inorg. Chem.* **1981**, *20*, 1192.
[35] CACAO program: C. Mealli, D. M. Proserpio, *J. Chem. Educ.* **1990**, *67*, 399.
[36] T. J. Kistenmacher, G. D. Stucky, *Inorg. Chem.* **1971**, *10*, 123.
[37] B. Bleaney, K. D. Bowers, *Proc. R. Soc. London Ser. A* **1952**, *214*, 451.
[38] P. Pyykkö, L. L. Lohr Jr., *Inorg. Chem.* **1981**, *20*, **1950**.
[39] N. J. Fitzpatrick, G. H. Murphy, *Inorg. Chim. Acta* **1984**, *87*, 41; *ibid.* **1986**, *111*, 139.